Epithelial-Restricted Gene Profile of Primary Cultures from Human Prostate Tumors: A Molecular Approach to Predict Clinical Behavior of Prostate Cancer

Simona Nanni,[1] Carmen Priolo,[1,5,6] Annalisa Grasselli,[1,4] Manuela D'Eletto,[1] Roberta Merola,[1] Fabiola Moretti,[1,5] Michele Gallucci,[1] Piero De Carli,[1] Steno Sentinelli,[1] Anna Maria Cianciulli,[1] Marcella Mottolese,[1] Paolo Carlini,[1] Diego Arcelli,[3] Mauro Helmer-Citterich,[3] Carlo Gaetano,[3] Massimo Loda,[6] Alfredo Pontecorvi,[1,2,4] Silvia Bacchetti,[1] Ada Sacchi,[1] and Antonella Farsetti[1,2,5]

[1]Departments of Experimental Oncology, Urology, Pathology, Clinical Pathology, and Medical Oncology and [2]Rome Oncogenomic Center, Regina Elena Cancer Institute; [3]Istituto Dermopatico dell'Immacolata; [4]Endocrinology, Catholic University; [5]INeMM, National Research Council, Rome, Italy and [6]Medical Oncology, Dana-Farber Cancer Institute, and Pathology, Brigham & Women's Hospital, Boston, Massachusetts

Abstract

The histopathologic and molecular heterogeneity of prostate cancer and the limited availability of human tumor tissue make unraveling the mechanisms of prostate carcinogenesis a challenging task. Our goal was to develop an *ex vivo* model that could be reliably used to define a prognostic signature based on gene expression profiling of cell cultures that maintained the tumor phenotype. To this end, we derived epithelial cultures from tissue explanted from 59 patients undergoing radical prostatectomy or cistoprostatectomy because of prostate benign hyperplasia/prostate cancer or bladder carcinoma. Patient selection criteria were absence of hormonal neoadjuvant treatment before surgery and diagnosis of clinically localized disease. Using this unique experimental material, we analyzed expression of 22,500 transcripts on the Affymetrix Human U133A GeneChip platform (Affymetrix, Inc., High Wycombe, United Kingdom). Cultures from normal/hyperplastic tissues with a prevalent luminal phenotype and from normal prostate epithelial tissue with basal phenotype (PrEC) served as controls. We have established a large number of prostate primary cultures highly enriched in the secretory phenotype. From them, we derived an epithelial-restricted transcriptional signature that (*a*) differentiated normal from tumor cells and (*b*) clearly separated cancer-derived lines into two distinct groups, which correlated with indolent or aggressive clinical behavior of the disease. Our findings provide (*a*) a method to expand human primary prostate carcinoma cells with a luminal phenotype, (*b*) a powerful experimental model to study primary prostate cancer biology, and (*c*) a novel means to characterize these tumors from a molecular genetic standpoint for prognostic and/or predictive purposes.

(Mol Cancer Res 2006;4(2):79–92)

Introduction

The clinical and pathologic features used for tumor staging include preoperative prostate-specific antigen (PSA) level, clinical stage, and degree of tumor differentiation (Gleason score) detected at biopsy (1-3). These variables can stratify patients into subgroups differing with respect to outcome after surgery and are widely used to guide clinical decision-making. Because of PSA-based cancer detection, patients are often presenting with PSA values and Gleason score within a low narrow range, suggesting an organ-confined disease. However, more than one-third of patients will relapse, showing that this is not always the case. Consequently, these variables are losing their discriminatory power, creating the need for novel diagnostic and prognostic markers.

Because the initiation and progression of prostate cancer involves multiple changes in gene expression, cDNA microarray technology has been recently used to identify disease-related gene expression patterns in prostate samples (4-8). This approach has detected alterations in several candidate genes associated with prostate cancer progression (9). However, there is not yet a definitive molecular classification that can predict consistently and reliably the clinical behavior of prostate cancer. Inconsistencies among reported prostate cancer gene expression signatures could be attributed at least in part to the fact that most of these analyses were done using bulk tissue samples that, in addition to neoplastic cells, contain

Received 7/18/05; revised 12/22/05; accepted 1/3/06.
Grant support: Associazione Italiana per la Ricerca sul Cancro, Ministero dell'Istruzione dell'Università e della Ricerca, and Ministero della Salute; Federazione Italiana Ricerca sul Cancro fellowship (S. Nanni); Associazione Italiana per la Ricerca sul Cancro regional grant (A. Pontecorvi); and DOD PC051271, NCI CA089021, Prostate Cancer Foundation (M. Loda).
The costs of publication of this article were defrayed in part by the payment of page charges. This article must therefore be hereby marked advertisement in accordance with 18 U.S.C. Section 1734 solely to indicate this fact.
Requests for reprints: Antonella Farsetti, Molecular Oncogenesis Laboratory, Department of Experimental Oncology, Regina Elena Cancer Institute-Experimental Research Center, Via delle Messi d'Oro 156, 00158 Rome, Italy. Phone: 39-6-5266-2531; Fax: 39-6-41805-26. E-mail: farsetti@ifo.it

doi:10.1158/1541-7786.MCR-05-0098

many other cell types, such as epithelial, stromal, endothelial cells and infiltrating lymphocytes. To circumvent this technical problem, we have analyzed RNA samples prepared from early passages of primary cultures highly enriched in epithelial cells that display a secretory phenotype and are derived from explants of prostate cancer tissue obtained at the time of surgery. The expression profile of the cancer cells consistently revealed elevated transcription of many genes known to be important in prostate carcinogenesis. These results have allowed us to identify an epithelial-restricted transcription profile that can be integrated with the grade and clinical information, with the aim of discriminating indolent and aggressive prostate tumors with histologically similar features.

Results

Isolation of Prostate Epithelial Cultures

To derive epithelial cultures from fresh samples of prostate, we collected surgical specimens from 59 patients undergoing radical prostatectomy or cystoprostatectomy because of benign prostatic hyperplasia, prostate cancer, or bladder carcinoma. These patients were selected from a total of 88 presenting to the Urology Division, Regina Elena Cancer Institute, between July 2002 and November 2003. Twenty-nine patients that received neoadjuvant hormonal treatment or had metastatic disease were excluded. The diagnosis and Gleason score were determined in each case by routine surgical pathology work-up. The characteristics of the study group are detailed in Table 1.

Tissue fragments were placed in growth medium and allowed to attach to the surface of culture dishes. From each prostate, samples were obtained from normal and tumor tissue. Small epithelial outgrowths appeared within 1 week exclusively from areas confirmed by histology to contain neoplastic tissue. In several cases of bilateral tumor, we obtained two cultures from the same patient. Only 1 of 8 samples (N1) of normal prostate (surgically removed because of bladder carcinoma) grew in culture, whereas we successfully derived two cell strains from benign prostatic hyperplasia (C10 and C17) and one from a contralateral normal tissue characterized by the presence of prostate intraepithelial neoplasia (C16sx). Cultures from normal/hyperplastic tissue (N1, C10, C17, and C16sx) and cancer had similar growth rate (10, 11). Importantly, all cultures had limited life span (20-25 population doublings) and similar cell morphology, as described (12). Cells were elongated and formed tight, cohesive islands (data not shown). Unlike normal and hyperplastic cells, cultures derived from tumors were capable of colony formation and anchorage-independent growth (Fig. 1A and B). As the tumor of origin, they exhibited loss of 8p21-22, a commonly deleted region in early-stage disease that includes the homeobox gene *NKX3.1* whose expression decreases with cancer progression (Fig. 1C; ref. 13). No such genetic alteration was detected in 4 of 4 nonmalignant prostate tissues (data not shown). In keeping with our selection of relatively early-stage carcinomas, fluorescence *in situ* hybridization analysis also revealed that prostate cancer tissues and cell strains had not undergone loss of PTEN or other genetic alterations commonly associated with more advanced disease (e.g., amplification of *MYC, EGFR*, or *AR*; Fig. 1C; refs. 9, 14-16).

Moreover, unlike normal or hyperplastic cells, prostate cancer–derived cells generally expressed telomerase (Fig. 1D; ref. 17). Evaluation of mRNA for the catalytic subunit hTERT [by quantitative real-time PCR (qRT-PCR)] and of telomerase activity (by telomeric repeat amplification protocol) was carried out in parallel on RNA or extracts from cultures at early passage (passages 2-8). hTERT mRNA was detected in most (24 of 27) of the samples regardless of their origin (benign versus malignant-derived cells), but expression levels were greatly variable. Telomerase activity was not detected in control populations, whereas it was present in the vast majority of tumor-derived cultures (prostate cancer) but to variable degrees. Although, as expected, cells lacking hTERT mRNA were negative by telomeric repeat amplification protocol, the reverse was not true because control populations were positive for mRNA but not enzymatic activity. Lastly, among samples positive for both mRNA and activity, there was no obvious quantitative interdependence between the two variables. Based on telomerase activity, approximately three subgroups of cultures could be identified, ranging from undetectable to intermediate to high level (defined by densitometry using an internal standard), with no apparent correlation with pathologic stage or Gleason score of the tumor of origin (see Table 1). Importantly, high levels of telomerase did not result in extension of cell life span.

Reactivation of hTERT and enzymatic activity has been proposed as a "diagnostic" marker in prostate cancer because it seems to be an early event in prostate carcinogenesis (18). Our results from a well-defined and selected population highly enriched in the epithelial phenotype confirm the usefulness of this marker in distinguishing between normal and tumor phenotypes.

Phenotype of Primary Prostate Epithelial Cell Cultures

Each normal epithelial cell type has a specific pattern of cytokeratin expression, which can be used as a differentiation marker (19). Cytospins of cultured cells were analyzed by immunocytochemistry using antibodies against several common prostate epithelial or stromal markers. The results were compared with the immunostaining pattern of commercial PrEC, a well-characterized transiently amplifying, basaloid population that exhibits partial secretory differentiation when reaching senescence (20). All cultures derived from tumors stained positive for the luminal cytokeratins CK8 (Fig. 2A) and CK18 (data not shown), AR, and PSA but were negative for p63 and HMwCK (Fig. 2A and C), a pattern consistent with a luminal/secretory phenotype. Consistent with the homogenous expression of epithelial markers, no staining was detected for the stromal markers vimentin or α-smooth muscle actin (Fig. 2A). Interestingly, expression of AR protein and PSA mRNA were modulated by treatment with DHT or the synthetic androgen (R1881), indicating that hormonal responsiveness was preserved (Fig. 2B). As expected, PrEC cells were positive for HMwCK and p63, weakly positive for CK8 (Fig. 2A), and negative for CK18 (data not shown), AR, and PSA (Fig. 2A and C, respectively). Nuclear estrogen receptor-β expression was seen in normal and transformed epithelial cells as well as in the original tissues, whereas

Table 1. Clinical and Pathologic Features of Patients and Tumors

Patients	Age	PSA (ng/mL)	Gleason Score Combined	Pathologic Stage (International Union Against Cancer 2002)	Tumor Site	Primary Cultures
T_1	71	5.4	9 (4 + 5)	$T_{3a}N_0M_x$	Left/right	C1sx and C1dx
T_2	61	11.7	7 (3 + 4)	$T_{3b}N_0M_x$	Left/right	C2dx
T_3	60	6.8	6 (3 + 3)	$T_{2a}N_0M_x$	Right	C3dx
T_4	67	5.2	8 (4 + 4)	$T_{3a}N_0M_x$	Left/right	—
T_5	71	5.2	7 (4 + 3)	$T_{2b}N_0M_x$	Left/right	—
T_6	51	2.1	5 (2 + 3)	$T_{3a}N_0M_x$	Left/right	—
T_7	61	6.2	7 (3 + 4)	$T_{2c}N_0M_x$	Left/right	—
T_8	67	18.5	7 (3 + 4)	$T_4N_0M_x$	Left/right	—
T_9	66	6.9	8 (4 + 4)	$T_{3b}N_0M_x$	Left/right	—
T_{11}	64	17.6	7 (3 + 4)	$T_{3b}N_0M_x$	Left/right	C11sx and C11dx
T_{12}	63	7	7 (4 + 3)	$T_{3b}N_0M_x$	Left/right	C12sx and C12dx
T_{13}	63	9.2	7 (3 + 4)	$T_{2a}N_0M_x$	Right	C13dx
T_{14}	71	4.3	7 (4 + 3)	$T_{2b}N_0M_x$	Left/right	C14sx and C14dx
T_{15}	64	8.3	6 (3 + 3)	$T_{2b}N_0M_x$	Left/right	C15sx and C15dx
T_{16}	60	11	7 (4 + 3)	$T_{3b}N_0M_x$	Right	C16sx* and C16dx
T_{18}	56	12	6 (3 + 3)	$T_{2a}N_0M_x$	Left/right	C18dx
T_{19}	67	13	7 (4 + 3)	$T_{3b}N_0M_x$	Left/right	C19sx and C19dx
T_{20}	63	8	4 (2 + 2)	NA		—
T_{21}	62	45.2	9 (4 + 5)	$T_{3b}N_0M_x$	Left/right	—
T_{22}	64	8	7 (3 + 4)	$T_{2c}N_0M_x$	Left/right	C22sx and C22dx
T_{23}	65	4.7	7 (4 + 3)	$T_{3b}N_0M_x$	Left/right	—
T_{24}	67	2.6	7 (3 + 4)	$T_{2b}N_0M_x$	Left/right	C24sx and C24dx
T_{25}	55	10.7	7 (4 + 3)	$T_{2c}N_0M_x$	Left/right	C25sx and C25dx
T_{26}	68	3.4	7 (3 + 4)	$T_{2c}N_0M_x$	Left/right	C26sx
T_{27}	66	6.7	7 (4 + 3)	$T_{3b}N_0M_x$	Right	C27dx
T_{28}	67	—	6 (3 + 3)	$T_{2c}N_0M_x$	Left/right	C28sx and C28dx
T_{29}	68	9.3	7 (3 + 4)	$T_{2c}N_0M_x$	Left/right	C29dx
T_{30}	59	11.6	Not measurable	$T_{2c}N_0M_x$		—
T_{31}	67	8.3	6 (3 + 3)	NA	Left/right	—
T_{32}	65	45.6	8 (4 + 4)	$T_{2b}N_0M_x$	Left/right	C32sx
T_{33}	66	13	7 (3 + 4)	$T_{2c}N_0M_x$	Left/right	C33sx and C33dx
T_{34}	57	6	6 (3 + 3)	$T_{2b}N_0M_x$	Left	—
T_{35}	62	5.8	7 (3 + 4)	$T_{2c}N_0M_x$	Left/right	C35sx
T_{36}	60	13	6 (3 + 3)	NA		—
T_{37}	67	13.1	8 (4 + 4)	$T_{2c}N_0M_x$	Left/right	C37sx and C37dx
T_{38}	55	23	7 (3 + 4)	$T_{2a}N_0M_x$	Right	C38dx
T_{39}	62	9.7	6 (3 + 3)	$T_{2c}N_1M_x$	Left/right	C39dx and C39sx
T_{40}	55	20.9	7 (4 + 3)	$T_{3a}N_0M_x$	Left/right	C40sx and C40dx
T_{41}	67	5.5	7 (3 + 4)	$T_{2c}N_0M_x$	Left/right	C41sx and C41dx
T_{42}	60	6.8	7 (3 + 4)	$T_{2b}N_0M_x$	Right	—
T_{43}	69	7.9	7 (3 + 4)	$T_{2c}N_0M_x$	Left/right	C43dx
T_{44}	50	25.9	7 (3 + 4)	$T_{2c}N_0M_x$	Left/right	—
T_{45}	67	19	7 (3 + 4)	$T_{3a}N_0M_x$	Left/right	C45
T_{46}	54	21	7 (4 + 3)	$T_{2c}N_0M_x$	Left/right	C46
T_{47}	64	7.8	7 (3 + 4)	$T_{2c}N_0M_x$	Left/right	—
T_{48}	57	11.6	7 (3 + 4)	$T_{2c}N_0M_x$	Left/right	C48
T_{49}	49	2.2	6 (3 + 3)	$T_{2a}N_0M_x$	Left/right	—
T_{50}	72	11.7	6 (3 + 3)	$T_{2b}N_0M_x$	Left/right	—
T_{51}	69	7.2	9 (4 + 5)	$T_{3b}N_0M_x$	Left/right	C51
10	64	6.1		Benign prostatic hyperplasia	—	C10
17	58	—		Benign prostatic hyperplasia	—	C17
N_1	61	—	—	—	—	N_1
N_2	65	—	—	—	—	—
N_3	58	—	—	—	—	—
N_4	67	—	—	—	—	—
N_5	66	—	—	—	—	—
N_6	69	—	—	—	—	—
N_7	61	—	—	—	—	—
N_8	58	—	—	—	—	—

NOTE: T_1-T_{51}, prostate cancer; N_1-N_8, normal prostate from patients with bladder carcinoma.
Abbreviation: NA, not available.
*Normal tissue + high-grade prostate intraepithelial neoplasia.

estrogen receptor-α was not detectable (data not shown). Of note, all these markers were preserved in immortalized cell lines we derived from primary cultures by transduction of both hTERT and SV40 T antigen genes.[7] Thus, the overall concordance of expression patterns between original tumors and cultured cells derivatives suggests that the phenotype of the tumor is preserved *in vitro*.

To date, no isolation of cells with all of the appropriate differentiation markers has been reported on such large scale, because most available culture models (21-23) consist of basal or transit amplifying cells.

[7] A. Farsetti et al., in preparation.

Gene Expression Profiling: Normal versus Prostate Cancer–Derived Cells

RNA was isolated from 22 tumor cultures and hybridized to Affymetrix Human U133A GeneChip arrays (Affymetrix, Inc., High Wycombe, United Kingdom). Because cultures representing matched case-controls could not be generated from normal prostate tissue adjacent or contralateral to the lesion, cultures derived from normal/hyperplastic tissues (N1, C10, C17, and C16sx) with a prevalent luminal phenotype and from normal prostate epithelial cells with the basal phenotype (PrEC) were used as controls.

Comparison of control versus tumor-derived populations (prostate cancer) was done using two different approaches for significance adjustments: Significance Analysis for Microarrays (SAM) and Max *T* test. In addition, Prediction Analysis for Microarrays (PAM) was used to classify categories and identify genes associated with prostate cancer (see Materials and Methods). The results from all three analysis, when compared, identified 89 common genes that were differentially expressed and discriminated between cancer and normal samples (Fig. 3A). Cluster analysis of these genes emerging from the intersection of PAM, SAM, and Max *T* test is shown in Fig. 3B. Among

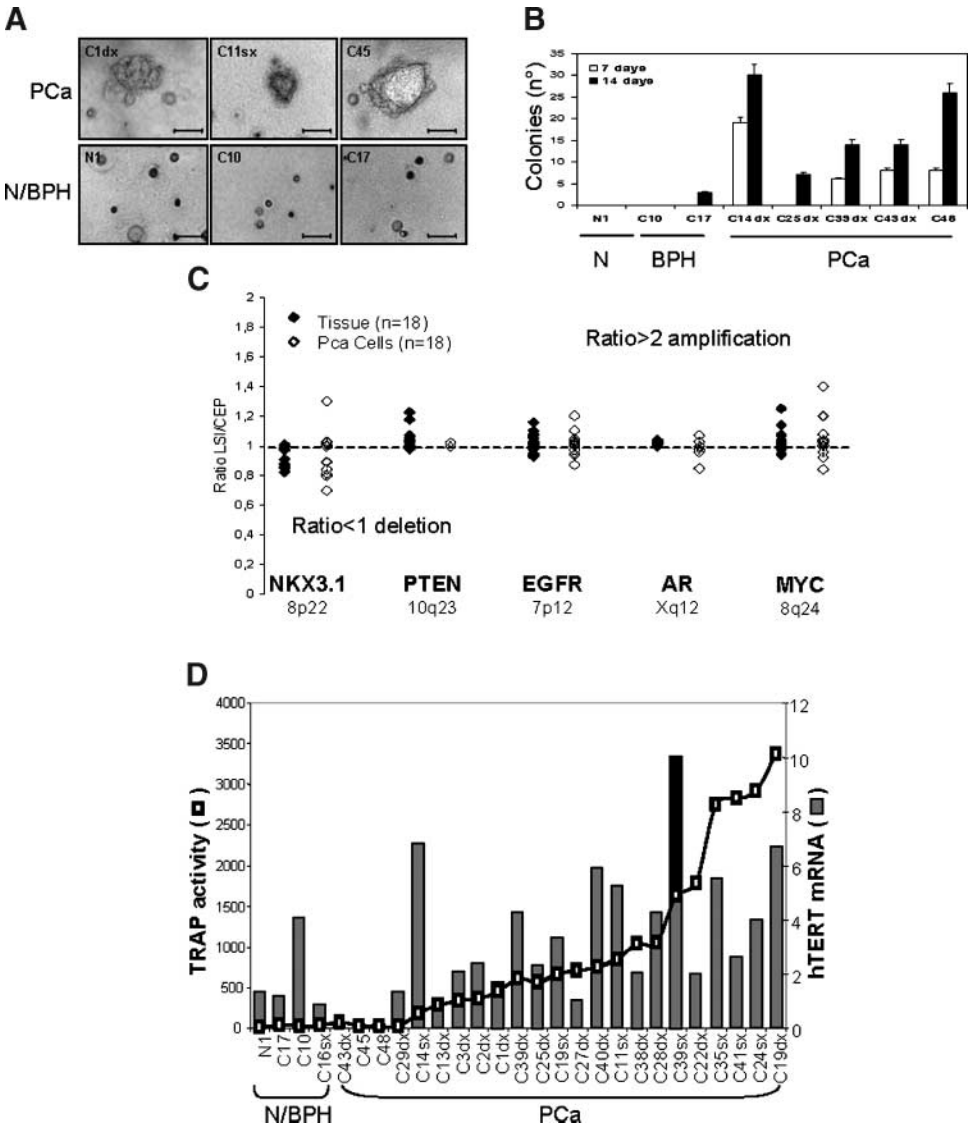

FIGURE 1. Phenotype of prostate cancer–derived cell strains. **A.** Anchorage-independent growth of prostate cancer (*PCa*) and normal/hyperplastic (*N/BPH*) cell strains observed at 3 weeks from plating. Primary cells derived from prostate cancer specimens (e.g., C1dx, C11sx, and C45) form colonies in soft agar. No colonies or only abortive colonies develop from cells derived from normal/hyperplastic tissue (N1, C10, and C17). All panels are of the same magnification. Bar, 200 μm. **B.** Colony formation by normal/hyperplastic and prostate cancer–derived cells at 7 and 14 days of growth. Columns, mean of two independent experiments done in triplicate; bars, SE. **C.** Fluorescence *in situ* hybridization. Distribution of ratios (gene signals/centromere; *LSI/CEP*) for *NKX3.1, PTEN, EGFR, AR*, and *MYC* genes in paraffin-embedded tissues (♦) and corresponding primary prostate cancer cells (◇). **D.** hTERT mRNA levels and telomerase activity in cell strains. Extracts from normal/hyperplastic and tumor derived cells (prostate cancer) were assayed for telomerase activity (□) by telomeric repeat amplification protocol (*TRAP*) assay in the presence of an internal control. Total activity was quantified by integrating the signal of the telomerase ladder, and relative activity was calculated as ratio to the internal standard. hTERT mRNA level (*columns*) was determined by qRT-PCR as described in Materials and Methods.

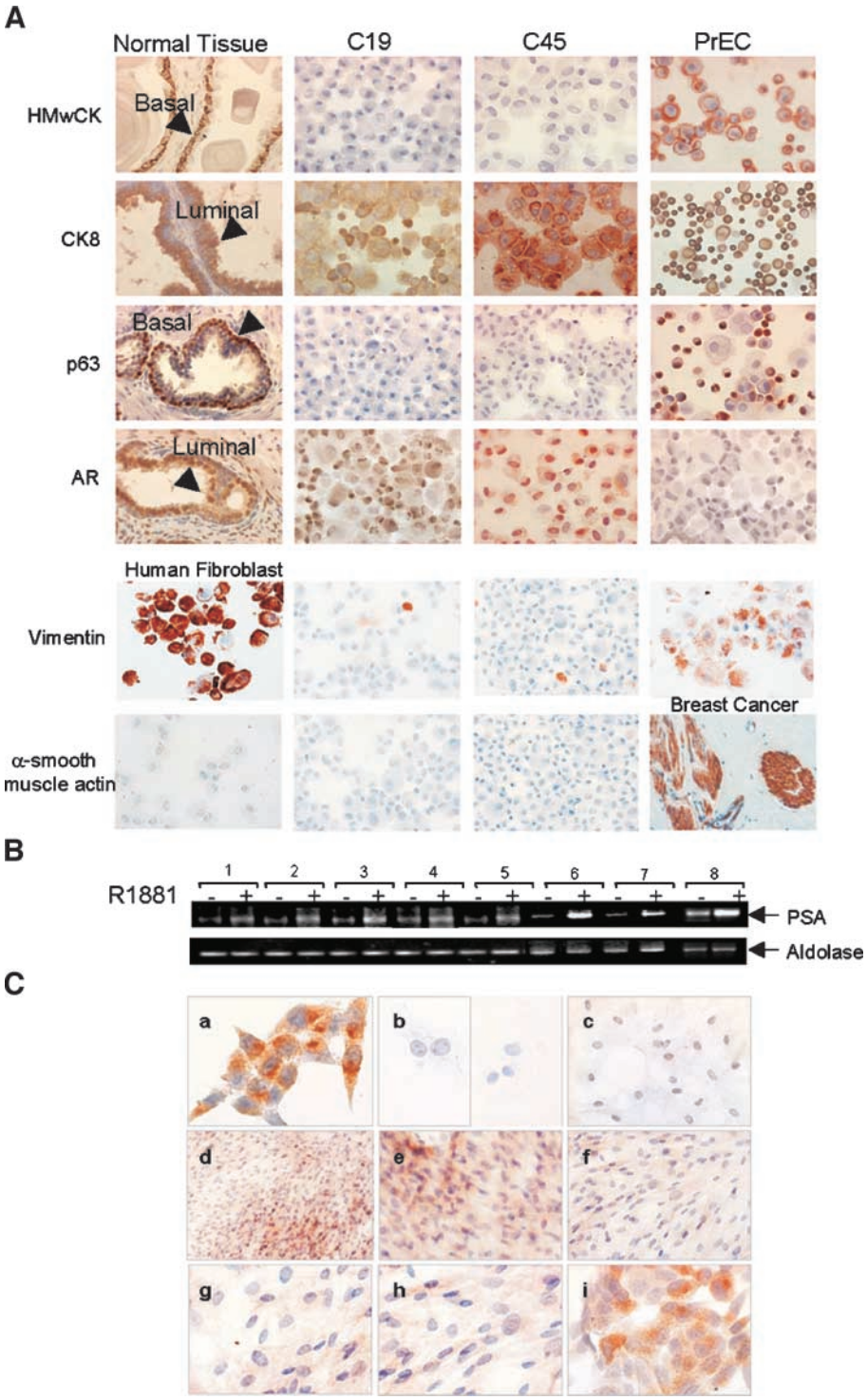

FIGURE 2. Epithelial immunophenotype and PSA expression of prostate cell strains. **A.** Immunohistochemical analysis of phenotypic markers of basal (*HMwCK* and *p63*) and luminal (*CK8* and *AR*) prostate epithelium and stromal compartment (*vimentin* and *α-smooth muscle actin*) done on normal prostate tissue sections (*normal tissue*), primary prostate cancer cells (*C19* and *C45*), and normal, commercially available, basaloid PrEC. Human primary fibroblast and breast cancer tissue were used as controls. Primary prostate cancer cells show a luminal epithelial phenotype expressing CK8 and AR but not p63, vimentin, and actin. PrEC express a basal-intermediate phenotype (positivity for HMwCK, CK8, p63, and vimentin). **B.** PSA mRNA levels observed in the presence or absence of androgen treatment (*R1881*). RT-PCR analysis of PSA was done on prostate cancer cell strains (*lanes 1-7*) and LNCaP cells (*lane 8*). The same RT-PCR conditions were used for the control housekeeping gene aldolase. **C.** PSA immunostaining in cell cultures derived from prostate cancer and normal tissues. a, LNCaP cells, positive control; b, PrEC (*left*) and human umbilical vascular endothelial cells (*right*), negative controls; c, N1 cells; d to i, prostate cancer–derived cells. Magnification, ×10 (*d*), ×20 (*e* and *f*), and ×40 (*g-i*). Primary prostate cancer cells show varying degrees of cytoplasmic staining for PSA.

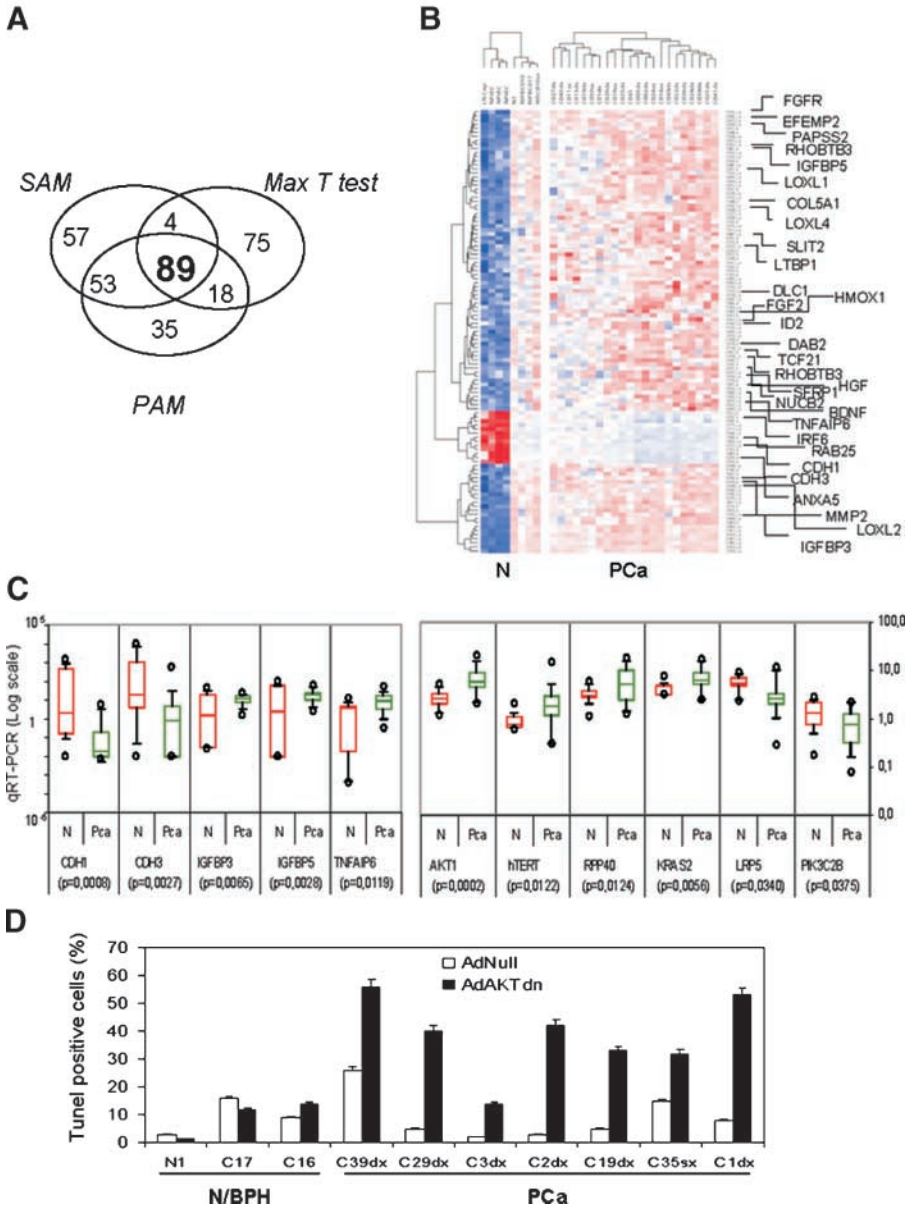

FIGURE 3. Molecular signature of prostate cancer, real-time PCR validation, and biological effect of dominant-negative AKT mutant. **A.** Supervised PAM, SAM, and Max *T* test analysis of normal versus tumor (prostate cancer)–derived cell cultures. **B.** Cluster analysis of the 89 genes derived from the intersection of PAM/SAM/Max T analysis. Right, genes with highest score in the intersection. The control populations were combined in a separate cluster because PrEC and LNCaP cells differ significantly in their gene expression pattern from primary cultures derived from normal/hyperplastic tissue or tumors (51, 52). **C.** Comparative qRT-PCR analysis of genes derived from intersected PAM/SAM/Max *T* test. mRNA levels from 22 cancer-derived cultures (prostate cancer) and 4 normal/hyperplastic cultures plus 3 different batches of commercial PrEC (*N*) are represented as box plots (see Materials and Methods) on logarithmic scale. ○, outliers. Student's *t* test *P*s. **D.** Normal/hyperplastic and prostate cancer cells were harvested after AdNull or AdAKTdn infection. Apoptotic cells were detected by terminal deoxunucleotidyl transferase–mediated dUTP nick end labeling (*TUNEL*) assay. Columns, mean percentage of apoptotic cells of two independent experiments, each done in duplicate; bars, SE.

the most differentially expressed transcripts (Fig. 3B), some were up-regulated in tumors [e.g., IGFBP5, IGFBP3, KRAS2, hTERT, two other molecules involved in telomere biology, TRF2 and TRF2IP (hRap1), and TNFAIP6], whereas others were down-regulated [e.g., E-cadherin (CDH1) and P-cadherin (CDH3)]. The expression of a subset of genes with the highest score was also validated by qRT-PCR (Fig. 3C). Among these, the serine/threonine kinase AKT/protein kinase B (AKT1), a key regulator of cell survival with a known role in prostate carcinogenesis (24), was highly overexpressed. We exploited this finding to investigate the role of AKT1 in the survival of seven prostate cancer–derived cells expressing high level of the wild-type protein and three normal/hyperplastic control cells. As shown in Fig. 3D, after infection with the AdAKTdn and on serum starvation, significant levels of apoptosis were detected in 6 of 7 prostate cancer–derived but not in control cell cultures.

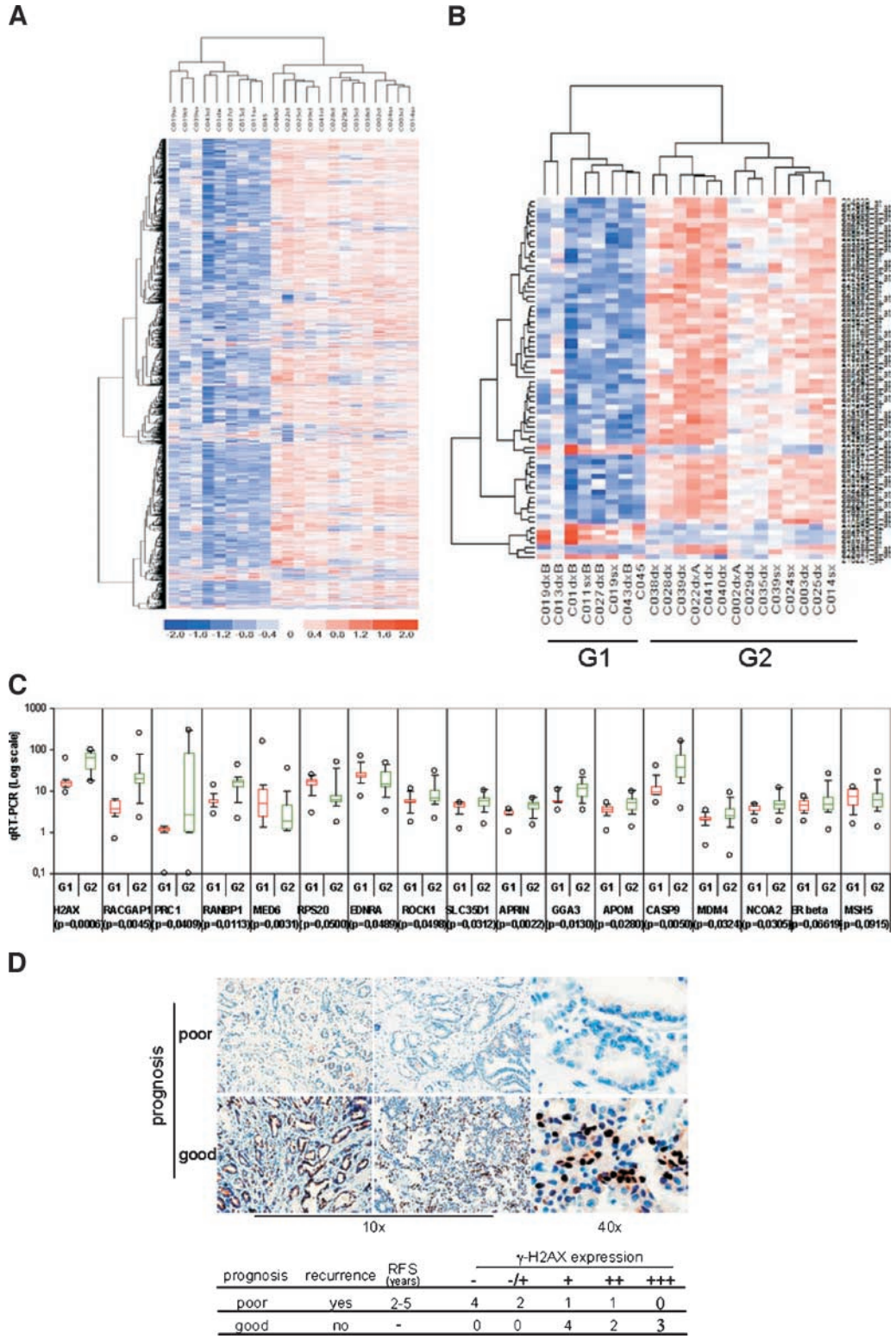

FIGURE 4. Gene expression patterns of prostate cancer–derived cells, real-time PCR validation, and H2AX phosphorylation levels in prostate cancer tissues. **A.** Unsupervised cluster analysis of 22 prostate cancer–derived cell cultures. **B.** Cluster analysis of 70 genes (listed in Table 3) derived from PAM and SAM intersection analyses done for the two groups of patients defined by recurrence status (see Table 2). **C.** Comparative qRT-PCR analysis of genes derived from intersected PAM/SAM or GO. Expression levels of the 22 prostate cancer–derived samples (G1 and G2 groups as in **B**) as in Fig. 3C. **D.** γ-H2AX protein expression was analyzed by immunohistochemistry (magnification, ×10 and ×40) on paraffin-embedded samples from an independent cohort of prostate cancer patients. Patients were divided in two groups according to their prognosis (poor or good). Bottom, table representing the distribution of patients according to γ-H2AX phosphorylation levels. RFS, relapse-free survival.

Table 2. Follow-up

No. Patients	Age	PSA (ng/mL)	Gleason score Combined	Pathologic Stage (International Union Against Cancer 2002)	Follow-up (mo)	Biochemical Recurrence	Biochemical Relapse-Free Survival	Second primary Neoplasia
1*	71	5.4	9 (4 + 5)	$T_{3a}N_0M_x$	40	Yes	6	Bladder
2*	61	11.7	7 (3 + 4)	$T_{3b}N_0M_x$	40	Yes	15	Hypopharynx
11	64	17.6	7 (3 + 4)	$T_{3b}N_0M_x$	38	Yes	19	Colon
19*	67	13	7 (4 + 3)	$T_{3b}N_0M_x$	33	Yes	6	
27*	66	6.7	7 (4 + 3)	$T_{3b}N_0M_x$	32	Yes	3	
45*	67	19	7 (3 + 4)	$T_{3a}N_0M_x$	24	Yes	7	
3	60	6.8	6 (3 + 3)	$T_{2a}N_0M_x$	40	No		
13	63	9.2	7 (3 + 4)	$T_{2a}N_0M_x$	36	No		
14	71	4.3	7 (4 + 3)	$T_{2b}N_0M_x$	36	No		
22	64	8	7 (3 + 4)	$T_{2c}N_0M_x$	33	No		
24	67	2.6	7 (3 + 4)	$T_{2b}N_0M_x$	32	No		
25	55	10.7	7 (4 + 3)	$T_{2c}N_0M_x$	32	No		
28	67	—	6 (3 + 3)	$T_{2c}N_0M_x$	32	No		
29	68	9.3	7 (3 + 4)	$T_{2c}N_0M_x$	31	No		
35	62	5.8	7 (3 + 4)	$T_{2c}N_0M_x$	31	No		
38	55	23	7 (3 + 4)	$T_{2a}N_0M_x$	31	No		
39	62	9.7	6 (3 + 3)	$T_{2c}N_1M_x$	30	No		
40*	55	20.9	7 (4 + 3)	$T_{3a}N_0M_x$	30	No		
41	67	5.5	7 (3 + 4)	$T_{2c}N_0M_x$	29	No		
43	69	7.9	7 (3 + 4)	$T_{2c}N_0M_x$	24	No		

*These patients were given radiotherapy following surgery.

Gene Profiling in Tumor Cell Populations

An additional important goal of our study was to find biomarkers that might predict disease outcome and biological response to therapy. To this end, we restricted the bioinformatic analysis to tumor-derived cell populations. Unsupervised cluster analysis of the 22,500 transcripts (displayed as a dendogram in Fig. 4A) divided the samples into two main groups.

Interestingly, samples derived from patients with poor outcome were clustered in the same group (Table 2). Further, a clear correlation was found between the transcriptional profile of the tumor cell strains and the clinicopathologic features of the original tumors, particularly with the pathologic stage, $pT_{3a/b}$ (extraprostatic extension and/or seminal vesicle invasion) and $T_{2a\text{-}c}$ (organ-confined disease), for the group with worse and better outcome, respectively.

We therefore did supervised SAM and PAM analyses of the groups defined by recurrence status to identify a prognostic expression signature. SAM/PAM intersection analysis resulted in 70 overlapping genes (listed in Table 3) out of 98 or 103, respectively. Cluster analysis of these genes also confirmed the presence of two main groups (termed G1 and G2 in Fig. 4B) similar (or substantially overlapping) to the groups defined by recurrence using supervised methods. Interestingly, the recurrence transcriptional profile, shared by two patients (13 and 43), which still exhibited the variables of an organ-confined disease, potentially allows to predict the worst outcome with a probability of 99% (Fisher's exact test). This may suggest that the epithelial-enriched gene profile represents an additional variable for the identification of tumors with poor prognosis based solely on tumor extension.

The prognostic expression signature revealed that, compared with the G2 group, G1 samples exhibit lower expression of genes involved in regulation of mitotic spindle elongation (e.g., PRC1) and in sensing DNA damage (e.g., H2AX). In contrast, a subset of genes usually associated with higher rate of proliferation, such as *RPS20, MED6, POLM*, and *POLL*, were overexpressed in G1 samples (Tables 3 and 4).

We next dissected *in silico* the functional class(es) of genes that mostly contribute to the G1 versus G2 signature. As shown in Table 4, the genes differentially expressed in the G1 cluster belong to many biological networks, among which the most relevant are (*a*) DNA replication, recombination, and repair; (*b*) RNA polymerase II transcription factor activity, and (*c*) positive regulation of cytosolic calcium ion concentration. Moreover, compared with the G2 cluster, the G1 signature showed relative lower expression of well-characterized genes, among which tumor suppressors, such as p53 (*TP53*) and Rb (*RB1*), and genes involved in the apoptosis pathway, such as *CASP9* and *CYCS*. Some of the most relevant genes emerging from the bioinformatic analysis (either SAM, PAM, or GOAL methods) were analyzed by qRT-PCR (Fig. 4C). Expression of 15 of 17 genes examined was found statistically different between the two clusters, thus confirming the accuracy of the microarrays analysis.

To validate *in vivo* the prognostic signature emerging from the cell populations, immunohistochemistry analysis was done on tissue samples derived from ours and from an independent set of 20 patients (17 with diagnosis of prostate cancer and 3 with benign prostatic hyperplasia; as detailed in Materials and Methods) exhibiting clinicohistopathologic features similar to our original cohort. The expression level of one of the most significant genes emerged from the transcription profile, histone H2AX, was evaluated in both cohorts with respect to the poor and good prognosis defined as relapse-free survival. Expression of the phosphorylated form of H2AX (γ-H2AX) was discriminating for the two groups of patients with distinct outcome both in our study (data not shown) and, as shown in Fig. 4D, in the independent retrospective cohort with a prolonged follow-up (12-14 years). No γ-H2AX staining was observed in the normal/hyperplastic samples (data not shown). The differential

Table 3. Intersect PAM-SAM Analysis of Recurrent versus Nonrecurrent Patients

Probe	Symbol	Description	PAM		SAM	
			Recurrent Score	Nonrecurrent Score	Score	Fold Change
207078_at	*MED6*	Mediator of RNA polymerase II transcription, subunit 6 homologue (yeast)	0.1513	0.0706	4.3346	2.0134
216247_at	*RPS20*	Ribosomal protein S20	0.1298	−0.0606	4.6127	1.7392
215597_x_at	*MYST4*	MYST histone acetyltransferase (monocytic leukemia) 4	0.1008	−0.047	4.4950	1.6697
218221_at	*ARNT*	Aryl hydrocarbon receptor nuclear translocator	0.0865	−0.0404	5.0695	1.4980
207971_s_at	*KIAA0582*		0.0518	−0.0242	3.9931	1.7469
202890_at	*MAP7*	Microtubule-associated protein 7	0.0246	−0.0115	4.0726	1.593
204712_at	*WIF1*	WNT inhibitory factor 1	0.007	−0.0032	4.0079	1.6129
201088_at	*KPNA2*	Karyopherin α2 (RAG cohort 1, importin α1)	−0.2943	0.1373	−4.1004	0.2438
209803_s_at	*PHLDA2*	Pleckstrin homology-like domain, family A, member 2	−0.2621	0.1223	−4.1166	0.3162
204026_s_at	*ZWINT*	ZW10 interactor	−0.2543	0.1187	−4.0063	0.2377
221505_at	*ANP32E*	Acidic (leucine-rich) nuclear phosphoprotein 32 family, member E	−0.2307	0.1077	−3.9218	0.2688
202673_at	*DPM1*	Dolichyl-phosphate mannosyltransferase polypeptide 1, catalytic subunit	−0.2262	0.1056	−4.2673	0.4208
222231_s_at	*PRO1855*		−0.2229	0.104	−4.4370	0.4575
201726_at	*ELAVL1*	ELAV (embryonic lethal, abnormal vision, *Drosophila*)–like 1 (Hu antigen R)	−0.196	0.0915	−3.9630	0.3919
218474_s_at	*KCTD5*	Potassium channel tetramerization domain containing 5	−0.1723	0.0804	−4.1733	0.4735
205381_at	*LRRC17*	Leucine-rich repeat containing 17	−0.1686	0.0787	−3.4661	0.2472
205436_s_at	*H2AFX*	H2A histone family, member X	−0.1681	0.0785	−3.8173	0.3566
201698_s_at	*SFRS9*	Splicing factor, arginine/serine-rich 9	−0.1514	0.0706	−4.4666	0.5692
222077_s_at	*RACGAP1*	Rac GTPase-activating protein 1	−0.1475	0.0688	−3.6721	0.3089
203324_s_at	*CAV2*	Caveolin 2	−0.1466	0.0684	−3.6064	0.2951
209025_s_at	*SYNCRIP*	Synaptotagmin binding, cytoplasmic RNA interacting protein	−0.1458	0.068	−3.8775	0.4286
201528_at	*RPA1*	Replication protein A1, 70 kDa	−0.1307	0.061	−3.8468	0.4596
221493_at	*TSPYL1*	TSPY-like 1	−0.1208	0.0564	−3.5656	0.3800
201760_s_at	*WSB2*	WD repeat and SOCS box-containing 2	−0.1109	0.0517	−3.5264	0.7506
209357_at	*CITED2*	Cbp/p300-interacting transactivator, with Glu/Asp-rich carboxyl-terminal domain, 2	−0.1104	0.0515	−3.4687	0.3005
208652_at	*PPP2CA*	Protein phosphatase 2 (formerly 2A), catalytic subunit, α isoform	−0.1086	0.0507	−3.8396	0.4780
202483_s_at	*RANBP1*	RAN-binding protein 1	−0.108	0.0504	−3.6861	0.4471
201317_s_at	*PSMA2*	Proteasome (prosome, macropain) subunit, α type, 2	−0.1069	0.0499	−3.9249	0.5264
202362_at	*RAP1A*	RAP1A, member of RAS oncogene family	−0.1065	0.0497	−3.8037	0.4907
201225_s_at	*SRRM1*	Serine/arginine repetitive matrix 1	−0.0955	0.0446	−3.6170	0.4707
212563_at	*BOP1*	Block of proliferation 1	−0.0905	0.0422	−4.0417	0.5373
219492_at	*CHIC2*	Cysteine-rich hydrophobic domain 2	−0.0887	0.0414	−3.5563	0.4294
209974_s_at	*BUB3*	Budding uninhibited by benzimidazoles 3 homologue (yeast)	−0.085	0.0397	−3.6481	0.4414
201277_s_at	*HNRPAB*	Heterogeneous nuclear ribonucleoprotein A/B	−0.0835	0.039	−3.7468	0.5025
202705_at	*CCNB2*	Cyclin B2	−0.0795	0.0371	−3.4869	0.3802
218611_at	*IER5*	Immediate early response 5	−0.0794	0.037	−3.4894	0.4191
208905_at	*CYCS*	Cytochrome *c*, somatic	−0.0792	0.0369	−3.5808	0.4334
205548_s_at	*BTG3*	BTG family, member 3	−0.0785	0.0367	−3.9618	0.5452
210211_s_at	*HSPCA*	Heat shock 90-kDa protein 1, α	−0.609	0.0284	−3.4283	0.4478
206055_s_at	*SNRPA1*	Small nuclear ribonucleoprotein polypeptide A′	−0.0588	0.0274	−3.3872	0.4072
212449_s_at	*LYPLA1*	Lysophospholipase I	−0.0588	0.0274	−3.3757	0.4109
212296_at	*PSMD14*	Proteasome (prosome, macropain) 26S subunit, non-ATPase, 14	−0.0566	0.0264	−3.4608	0.4668
203349_s_at	*ETV5*	Ets variant gene 5 (ets-related molecule)	−0.0541	0.0253	−3.5119	0.4699
204094_s_at	*TSC22D2*	TSC22 domain family 2	−0.0529	0.0247	−3.6648	0.522
208901_s_at	*TOP1*	Topoisomerase (DNA) I	−0.0524	0.0245	−3.7964	0.5571
213154_s_at	*BICD2*	Bicaudal D homologue 2 (*Drosophila*)	−0.0516	0.0241	−3.4680	0.4488
202043_s_at	*SMS*	Spermine synthase	−0.0512	0.0239	−3.3937	0.4141
212918_at	*FLJ22028*		−0.0492	0.023	−3.4142	0.4320
217919_s_at	*MRPL42*	Mitochondrial ribosomal protein L42	−0.0481	0.0225	−3.6327	0.5117
201388_at	*PSMD3*	Proteasome (prosome, macropain) 26S subunit, non-ATPase, 3	−0.0464	0.0216	−3.7725	0.5733
208374_s_at	*CAPZA1*	Capping protein (actin filament) muscle Z-line, α1	−0.0459	0.0214	−3.5372	0.5036
201821_s_at	*TIMM17A*	Translocase of inner mitochondrial membrane 17 homologue A (yeast)	−0.0441	0.0206	−3.6381	0.5316
202078_at	*COPS3*	COP9 constitutive photomorphogenic homologue subunit 3 (*Arabidopsis*)	−0.0428	0.02	−3.6500	0.5445
203910_at	*PARG1*	PTPL1-associated RhoGAP1	−0.0427	0.0199	−3.3551	0.4777
218982_s_at	*MRPS17*	Mitochondrial ribosomal protein S17	−0.0426	0.0199	−3.5872	0.5147
218156_s_at	*FLJ10534*		−0.0354	0.0165	−3.4077	0.4613
202352_s_at	*PSMD12*	Proteasome (prosome, macropain) 26S subunit, non-ATPase, 12	−0.035	0.0164	−3.5635	0.5134
208152_s_at	*DDX21*	DEAD (Asp-Glu-Ala-Asp) box polypeptide 21	−0.0338	0.0158	−3.3644	0.4788
200627_at	*TEBP*	Prostaglandin E synthase 3 (cytosolic)	−0.0326	0.0152	−3.6390	0.5406
202693_s_at	*STK17A*	Serine/threonine kinase 17a (apoptosis-inducing)	−0.0318	0.0148	−3.4759	0.4828
212502_at	*C10orf22*	Chromosome 10 open reading frame 22	−0.0266	0.0124	−3.6106	0.5437
200712_s_at	*MAPRE1*	Microtubule-associated protein, RP/EB family, member 1	−0.0257	0.012	−3.4970	0.5179
203109_at	*UBE2M*	Ubiquitin-conjugating enzyme E2M (UBC12 homologue, yeast)	−0.0228	0.0106	−3.5711	0.5394
204839_at	*POP5*	Processing of precursor 5, RNase P/MRP subunit (*Saccharomyxes cerevisiae*)	−0.018	0.0084	−3.6761	0.5663
201672_s_at	*USP14*	Ubiquitin specific protease 14 (tRNA-guanine transglycosylase)	−0.017	0.0079	−3.3218	0.5639
210949_s_at	*EIF3S8*	Eukaryotic translation initiation factor 3, subunit 8, 110 kDa	−0.0152	0.0071	−3.6089	0.5553
201175_at	*TMX2*	Thioredoxin-related transmembrane protein 2	−0.0142	0.0066	−3.6734	0.5660
221568_s_at	*LIN7C*	Lin-7 homologue C (*Caenorhabditis elegans*)	−0.014	0.0065	−3.4589	0.5106
212129_at	*NIPA2*	Nonimprinted in Prader-Willi/Angelman syndrome 2	−0.0119	0.0056	−3.7737	0.6003
217769_s_at	*C13orf12*	Chromosome 13 open reading frame 12	−0.0067	−0.0029	−3.6372	0.5842

Table 4. GO Analysis of Recurrent versus Nonrecurrent Patients

Functional Class	Genes
Nucleus/cytokinesis/kinetochore/mitosis and cell cycle/microtubule cytoskeleton organization and biogenesis	*BUB3, BUB1, BUB1B, KIF4A, KIF22, BTG3, CCNB1, CCNB2, CCNG2, CDK2, CDC2, TERF1, RAD21, CDC6, CDC25A, KNTC1, POLS, ANAPC1, CENPF, CNPE, CENPA, ZW10, ZWINT,* ***MAP7****, MAPRE1, SUMO3, STK6, KTNC2, PLK1*
Membrane/integral to membrane/voltage-gated potassium channel complex/calcium-dependent cell-cell adhesion	*LIN7C, CAV2, CAV1, CAV3, TIMM17A, TIMM17B, TIMM44, KCTD5,* ***DCHS1, DSG1, PCDHB6****, TNFAIP1*
Proteasome complex ubiquitin conjugating enzyme activity/ubiquitin-dependent protein catabolism	*PSMD12, PSMD3, PSMD14, PSMA2, PRES, PSMD4, PSMC4, PSMC3, PSMD5, P4410, USP5, USP14, UBE2M, UBE2V2, USP2*
DNA binding, metabolism, replication, repair/nuclear pore	*ANP32E, KPNA2, KPNA1, NBST, ERCC5, ERCC1, XRCC5, ATR, PARP1, PCNA, ERCC8, HMGB1, HMGB2, HMGA1, RAD51, RAD1, APEX1,* ***POLM, POLL, POLB, MSH5, MSH6****, XPA, FEN1, DDB1, RAD50, RAD21, RAD17, RAN, TOP1, TOP3A, RB1, BRCA1, PHB*
RNA catabolism, splicing, processing, binding, cap binding, helicase activity	*ELAVL1, BOP1, PPP2CA, SFRS9, POP5, POP4, LSM4, NCBP1, NCBP2, NCBP1, RNUT1, CUGBP1, HNRPA1, HNRPD, SYNCRYP, SNRPA1, ZNF638, RRAGC, DDX21, DDX9, PIAS1, G3BR, ASCC3L1*
Positive regulation of cytosolic calcium ion concentration	***PLCE1, EDNRA, EDG2, CCR1, GPR24***
Mitochondrial small ribosomal subunit	*MRPS17, MRPS15, MRPS18A, MRPS18B, MRPS16, MRPS28, MRPS33, MRLP42*
Caspase activation via cytochrome *c*	*CASP9, TP53, CYCS, DIABLO, STK17A*
Cell-cell signaling/receptor activity intracellular signaling cascade	***WIF1, MED6, IGF1R, TGFBR3,*** *RACGAP1, RSU1*
RNA polymerase II transcription factor activity, enhancer binding	***TFAP2A, PURA, NR5A2, RFX3, EPAS1, ATBF1, HIF1A, ARNT, IRF8, CEBPA****, TRIP13, NFX1*
Rho-protein signal transduction	*PARG1, ARHGDIA, LIMK1, ROCK1, CLF1, RHOG, RHOA, TSC1*

NOTE: Genes up-regulated in G1 versus G2 are in bold; genes altered also in the intersect PAM/SAM analysis are underlined.

expression of γ-H2AX detected in the good and poor outcome groups provides a clear correlation between *in vitro* and *in vivo* data. These findings are promising, as they support the possibility that the expression pattern of individual genes may contribute in the future to optimize patients' stratification and prognosis.

Discussion

We have developed an *ex vivo* model that can be reliably used to define, at diagnosis, a prognostic signature based on gene expression profiling of short-term cultures of prostate carcinoma cells. The methodology we describe overcomes the heterogeneity of clinical samples commonly employed in gene profiling studies and provides sufficient material for detailed characterization of primary prostate tumors. Although primary epithelial cells are commonly cultured in defined medium with no or low serum, our cultures were isolated and maintained in 20% serum. This condition has been proven to greatly favor rapid outgrowth of tumor cells from fragments of prostatectomy specimens. These cells maintain the secretory phenotype of the original tumor. Specifically, they express PSA and AR, the most relevant differentiation markers of the luminal compartment of prostate epithelium, and maintain androgen responsiveness (Fig. 2; data not shown). This immunophenotypic concordance with tumor tissue was preserved also in immortal lines derived from the primary cells, a feature that greatly facilitates their use as indicators of tumor responsiveness to treatment. In conclusion, our cultures represent a powerful experimental system for the study of primary prostate cancer biology with relevant clinical implications.

From the prostate cell lines, we obtained an epithelial-restricted gene expression profile. These signatures reliably and consistently differentiated between cells derived from normal tissue and from prostate cancer. Thus, the tumor transcription pattern is essentially maintained in culture. Previously, a similarity in gene expression profiling was noted between primary breast tumors and their epithelial cell derivatives (25). Our analysis confirms the gene expression patterns of previous studies on prostate cancers (4, 5, 26) but also identifies additional genes whose expression is specifically altered in the secretory prostate epithelium (i.e., components of the telomere complex, such as hTERT, TRF2, and TRF2IP). In particular, the gene profile we describe allows stratification of cell lines (and thus of patients) and therefore the possibility of exploiting the cells for *ex vivo* targeted therapies as exemplified by our induction of apoptosis through functional inhibition of AKT (27). Inhibitors of the phosphatidylinositol 3-kinase/AKT pathway are currently being evaluated as anticancer agents in prostate cancer clinical trials (28, 29), and other pathways could be similarly targeted with appropriate drugs. In this regard, among the 89 genes emerging from the intersection of the normal versus cancer analyses (Fig. 3), we found a specific up-regulation of the *HMOX1* gene in the cancer-derived population, confirming again a strong involvement of the phosphatidylinositol 3-kinase signaling and downstream effectors in prostate cancer, in agreement with previous reports (30).

The clear distinction between tumor and normal samples prompted us to focus on the tumor cell populations to obtain information that would add to clinical and pathologic variables and thus help in selecting the most appropriate therapy and improve prognosis. The supervised bioinformatics analysis clearly highlighted two distinct transcriptional signatures. Of these, the one marking the G1 cluster (Fig. 4B) was specifically associated with a more severe clinical course of

the disease within a follow-up ranging from 24 to 40 months (see Table 2). Indeed, we found a significant correlation between this transcriptional signature and the pathologic stage, particularly the extension of the lesion. Of note, two patients with organ-confined disease (patients 13 and 43; see Table 2) exhibit the signature of aggressive tumors. In this respect, the transcriptional profile we identified might help to predict recurrence in patients that do not display features of aggressive biological behavior as assessed by traditional clinicopathologic variables.

With very few exceptions, what emerged from the gene profile restricted to the cancer-derived cells and from the qRT-PCR analysis of a set of genes with the highest discriminating score is a clear pattern of progressive down-regulation of expression that follows the progression of the disease. One of the striking features of the profile associated with poor prognosis is in fact a relatively lower expression of genes (identified by GOAL analysis; Table 4) belonging to families controlling cell cycle, mitosis, and DNA repair. Two recent studies (31, 32) have reported that the DNA damage response is activated in preneoplastic lesions and down-regulated with disease progression and suggested that the initial activation of DNA repair represents one of the earliest barriers to cancer, such that loss of this pathway facilitates acquisition of malignant properties. Our findings agree with this concept. Indeed, the vast number of down-regulated genes involved in DNA damage sensing and repair, among which are "early sensor," such as H2AX (Table 3; Fig. 4), indicates that these pathways are severely compromised or even abrogated in the G1 group. To our knowledge, this is the first evidence of a potential prognostic role of the H2AX expression in prostate cancer. Validation of these data on *in vivo* samples derived from ours and from an independent set of patients strongly supports this conclusion, although a prolonged follow-up for our cohort and analysis of additional genes belonging to the prognostic signature are required.

The G1 signature comprises also few up-regulated genes, among which are those that contribute to augment transcriptional activity (*MED6*) and promote cell proliferation (*RPS20*). The enhanced expression of *MED6*, confirmed also by qRT-PCR (Fig. 4C), in the bad prognosis G1 group, compared with the G2 group, is particularly intriguing, because this gene is known to play a key role in the activation of the basal transcription machinery (33). In agreement with previous gene profiling reports (34), we found higher expression of *EDNRA* in the G1 compared with the G2 groups. This finding supports recent reports (28) that propose EDNRA antagonists, such as atrasentan, for therapeutic intervention in prostate cancer.

It is notable that within the G1 prognostic signature we observed induction of genes involved in the activation of cellular response to hypoxia, such as *HIF1α, HIF2α* (*EPAS1*), and *HIF1β* (*ARNT*; Tables 3 and 4). Because tumor hypoxia and overexpression of the hypoxia-inducible factors pathway have been associated with resistance to certain therapies (35), the information deriving from our prognostic signature acquires an additional value in terms of optimization of patient stratification and outcome-prediction.

In conclusion, short-term cell cultures derived from primary prostate tumors yield sufficient material that is devoid of contaminating nonepithelial cells and is amenable to extensive molecular characterization. This methodology may lead to the further identification and refinement of expression signatures that may guide therapeutic options in prostate cancer.

Materials and Methods

Tissue Samples

Fresh samples of tumoral, hyperplastic, and normal prostate tissues were obtained after informed consent from 49 patients undergoing radical prostatectomy for clinically localized prostate cancer, 2 patients undergoing transurethral resection of the prostate for benign prostatic hyperplasia, and 8 patients undergoing cystoprostatectomy for bladder carcinoma. None of the cancer patients had received neoadjuvant hormonal treatment or radiotherapy. Surgical specimens were dissected from a qualified pathologist within 1 hour of surgery and used for histopathologic examination, Gleason score evaluation, and immunohistochemical staining. Staging was done in accordance with the International Union Against Cancer 2002 tumor-node-metastasis system.[8] Small tissue samples were used to isolate primary cell cultures, and frozen sections were used to confirm the diagnosis of each specimen. Clinical and pathologic characteristics of patients and surgical specimens are illustrated in Table 1. A retrospective analysis was done on an independent cohort of 20 patients (17 Prostate cancer and 3 benign prostatic hyperplasia) that had undergone radical prostatectomy at the Urology Division, Regina Elena Cancer Institute, between September 1991 and December 1993. These patients represent a homogenous group with clinical and histopathologic variables comparable with those of our study cohort and were selected using the same exclusion criteria. Their characteristics are as follows: age range, 41 to 73 years; PSA range, 5.6 to 12.3 ng/mL; Gleason score range, 6 (3 + 3) to 10 (5 + 5); and tumor-node-metastasis range, pT_{2b}-pT_{3b}, according to International Union Against Cancer 2002.

Primary Cultures

Horizontal sections (5 mm thick) of prostate tissue were transported to the laboratory in ice-cold Iscove's modified Dulbecco's medium (Invitrogen, Carlsbad, CA) supplemented with 20% fetal bovine serum (Hyclone, Logan, UT) and glutamine, and cultures were started within 2 to 3 hours of surgery. Prostate samples were chopped into small fragments of 1 to 2 mm^3 with sterile scissors and placed in 35-mm dishes containing growth medium. The explants were incubated at 37°C in a humidified 5% CO_2 atmosphere to allow attachment to the culture dish (1 week) and epithelial cell growth. As cells reached confluence, they were detached by both trypsin/EDTA mixture and mechanical means and passaged at a split ratio of 1:4. At near confluence, cells aliquots of the primary cultures were frozen and stored in liquid nitrogen. For serial passages, routine trypsinization was used and the split ratio of the cells was 1:4.

[8] International Union Against Cancer. TNM classification of malignant tumors. 6th ed. New York: Wiley-Liss; 2002.

Cell Lines

Prostate epithelial cells (PrEC) were cultured according to the manufacturer's protocols (Cambrex BioScience, Verviers, Belgium). Human prostate cancer cell lines (LNCaP) were cultured in RPMI 1640 supplemented with 10% fetal bovine serum (Invitrogen), 4.5 g/L glucose, and 0.1 mol/L HEPES. Human primary fibroblast were cultured in DMEM with 10% donor serum (Invitrogen).

Soft Agar Assay

Cells (2×10^5) were resuspended in 1 mL of 0.4% agar Noble (Difco Laboratories, Kansas City, MO) in complete Iscove's modified Dulbecco's medium and seeded into to 35-mm dish coated with 0.6% agar Noble in the same medium. Every 3 days, 0.5 mL fresh medium was added. After 2 to 3 weeks, cells were stained with 0.4 mg/mL neutral red, and anchorage-independent growth was assessed by counting colonies of >200 μm in diameter.

Clonogenicity Assay

Cells ($n = 200$) were seeded in duplicate in six-well plates in complete Iscove's modified Dulbecco's medium. After 7 to 14 days, cells were fixed and stained with 0.5% crystal violet and colonies were counted.

Fluorescence In situ *Hybridization Analysis*

The procedure for fluorescence *in situ* hybridization has been described previously (36). Briefly, the Vysis (Downers Grove, IL) ProVysion multicolor mixture was used for detection of *AR* (Xq12), *EGFR* (7p12), *PTEN* (10q23), *NKX3.1* (8p22), and *MYC* (8q24) genes, and chromosome numeration probes specific for X, 7, 8, and 10 chromosomes were used to adjust for aneuploidy and to establish the presence of deletions/amplifications. Centromeres and specific gene regions copy numbers were counted in at least 100 cells. The ratios between specific-gene and centromeric copy number were calculated to establish the presence of amplified (*AR, MYC*, and *EGFR*) or deleted (*PTEN* and *NKX3.1*) genes.

Telomeric Repeat Amplification Protocol Assay

Cell extracts were assayed for telomerase activity by the telomeric repeat amplification protocol (37). Telomerase activity was normalized to an internal standard and quantified by densitometric analysis with NIH Image J. 24 software as described (38).

RNA Extraction and RT-PCR

Cells were cultured in the presence or absence of methyltrienolone (R1881; gift from A. Banhiamad, Jena University, Germany) for 72 hours as described by Nanni et al. (38). Cells were homogenized in Trizol (Invitrogen) and total RNA was isolated according to the manufacturer's instructions. cDNA preparation and PCR conditions were as described previously (38). PSA and aldolase primers were used as described (38, 39).

Real-time PCR Analysis

cDNA synthesis was done from two independent RNA preparations using SuperScript III Platinum Two-Step qRT-PCR kit (Invitrogen) and High-Capacity cDNA Archive kit (Applied Biosystems, Foster City, CA) and qRT-PCR was done with the ABI Prism 7500 PCR instruments (Applied Biosystems) to amplify samples in triplicate. Predesigned TaqMan primers and probe (Applied Biosystems) specific for estrogen receptor-β1, H2AX, MDM4, MSH5, 18S rRNA, and RNase P were used. qRT-PCR was done using SYBR Master mix (Applied Biosystems) with evaluation of dissociation curves. hTERT and AKT1 primers were described previously (38, 40). For the remaining genes, specific, intron spanning, primers were designed using Primer Express 2.0 (Applied Biosystems). Primers were as follows: APOM forward 5′-CCGATGCAGCTCCACCTT-3′ and reverse 5′-AGTCAGGTGGTAGATCCATTTCC-3′, APRIN forward 5′-GCCTACAAATCCTTTCCTGGAA-3′ and reverse 5′-GAGCACTGATAGATTCGGTATCTATGTG-3′, CASP9 forward 5′-GAGGTTCTCAGACCGGAAACAC-3′ and reverse 5′-CATTTCCCCTCAAACTCTCAAGA-3′, CDH1 forward 5′-CCAGAAACGGAGGCCTGAT-3′ and reverse 5′-CTGGGACTCCACCTACAGAAAGTT-3′, CDH3 forward 5′-CAGGGAGGCTGAAGTGACCTT-3′ and reverse 5′-GAAGTCATCATTATCAGTGCTAAACAGA-3′, EDNRA forward 5′-CAGAAGGAATGGCAGCTTGAG-3′ and reverse 5′-CACTTCTCGACGCTGCTTAAGA-3′, GGA3 forward 5′-GCCAGAAGAAGCAAAGATCAAAG-3′ and reverse 5′-TGGTGGGTCAGACTGCACTATG-3′, KRAS2 forward 5′-CCCAGGTGCGGGAGAGA-3′ and reverse 5′-CTACGCCACCAGCTCCAACT-3′, IGFBP3 forward 5′-AGTCCAAGCGGGAGACAGAA-3′ and reverse 5′-GGTGATTCAGTGTGTCTTCCATTT-3′, IGFBP5 forward 5′-CTACCGCGAGCAAGTCAAGAT-3′ and reverse 5′-TGTTTGGGCCGGAAGATC-3′, LRP5 forward 5′-AACATGATCGAGTCGTCCAACA-3′ and reverse 5′-GATATAATCGCTGTACTGCGTCAGA-3′, MED6 forward 5′-TGGTCAAAATGCAGAGGCTAAC-3′ and reverse 5′-TCTTGAGCATGCAAAAGGATGT-3′, NCOA2 forward 5′-TGTTGCTGCACAAACGAAGAG-3′ and reverse 5′-GGCTTCCCCATCGTTTGTC-3′, PIK3C2B forward 5′-CCGCATCCCCATCATCTG-3′ and reverse 5′-GCTGAGGGAGCAGGAGAGGTA-3′, PRC1 forward 5′-GGAGCGTCCGCCATGAG-3′ and reverse 5′-CCGAAGGTGATTTAGGGCTTTC-3′, RACGAP1 forward 5′-GTCATGGAATTTAAGTGATTTACTGAAGA-3′ and reverse 5′-GCACAAGCTGCTCAAACAGATT-3′, RANBP1 forward 5′-CTGGAAGAAGATGAAGAGGAACTTTT-3′ and reverse 5′-CCTTCCATTCTGGGAGATCGT-3′, ROCK1 forward 5′-AGAATTGGATGAAGAGGGAAATCA-3′ and reverse 5′-CTTTTCTTTGGTACTCATTAATTCTATGCT-3′, RPP40 forward 5′-GGTTCAGAAGAATCGACAATGATG-3′ and reverse 5′-ACGTGCTCAGTGCTACTTTTGG-3′, slc35d1 forward 5′-GCCCACCCTGGCCATT-3′ and reverse 5′-TCAGCCCAGCCTTCAAACTC-3′, and TNFAIP6 forward 5′-GCGGCCATCTCGCAACT-3′ and reverse 5′-TCCAGCAGCACAGACATGAAA-3′.

The mRNA of each gene was quantified using the Standard Curve Method (5-log dilutions in triplicate) and expressed relative to the 18S rRNA or RNase P. Data are represented as box plots generated from Excel charts and plotted on a log scale. In this display, data are represented as boxes showing medians and upper and lower quartiles.

Whiskers indicate minimum and maximum values, excluding the outliers that are directly depicted in each graph.

Antibodies

The following monoclonal antibodies were used: 34βE12 anti-HMWCK, 28A4 anti-PSA, 6F11 anti–estrogen receptor-α, and PPG5/10 anti-estrogen receptor-β (all from UCS Diagnostic S.r.l., Rome, Italy); 35βH1 anti-CK8, AR441 anti-AR, V9 anti-vimentin, and 1A4 α-smooth muscle actin (Dako, Carpinteria, CA); 4A4 anti-p63 (Neomarker-LabVision Corp., Carpinteria, CA); anti-phospho-histone H2AX, Ser^{139} (Upstate, Lake Placid, NY).

Immunoperoxidase Assay on Tissue Samples and Cell Cultures

Sections (5 μm) of paraffin-embedded tissues were deparaffinized and rehydrated in decreasing ethanol concentrations. Antigen retrieval was done by heating at 96°C for 15 minutes in 10 mmol/L citrate buffer (pH 6.0). Endogenous peroxidase was quenched with 3% H_2O_2 in 60% methanol, and nonspecific binding was blocked by a 10-minute incubation with normal serum (ScyTek Laboratories, Logan, UT). Samples were then incubated with the primary antibody for 1 hour in a humidified atmosphere. Detection steps were done using the UltraTek HRP kit (ScyTek Laboratories), and peroxidase activity was localized with 3,3′-diaminobenzidine/H_2O_2 substrate (Dako). Slides were counterstained with hematoxylin, rehydrated, and mounted for microscopic examination. Immunocytochemical analysis was done on cytospins (400 rpm for 5 min) fixed for 30 minutes in formalin. Cells were treated and immunoperoxidase stained as described above for tissue sections. PSA immunostaining was done on cells grown on chamber slides (Lab-Tek, Naperville, IL).

Gene Expression Profiling

Total cellular RNA was isolated by using RNeasy kits (Qiagen, Germantown, MD). Preparation of labeled cRNA and hybridization (GeneChip Human Genome U133A 2.0 Array; Affymetrix) was done according to the Affymetrix GeneChip Expression analysis manual. Microarray data have been deposited in the Gene Expression Omnibus under accession no. GSE3868 (submitted by A. Farsetti).

Data Analysis

Affymetrix GeneChip scanning was analyzed by customized R language–based script (see http://www.r-project.org) using the Bioconductor packages (see http://www.bioconductor.org) for quality-control analysis, data normalization, hierarchical cluster, and identification of differentially expressed transcripts. Specifically, the gcrma package was used for chip normalization and background correction; the vsn package provided calibration and transformation of the probe intensities to evaluate the within-group and between-group variabilities. The genefilter package was used to separate genes with high variance according to the interquartile range method. Unsupervised two-way (genes against samples) hierarchical clustering method using the about (3,000) probe set of our data set, previously filtered, was used to test the internal consistency, to explore the relationship among samples, and to check if the individual samples clustered together according to their features. The unsupervised cluster analysis was followed by two similar tests, SAM and mt.MaxT function (Max T test), to identify genes that distinguished between two categories (normal versus cancer and/or recurrent versus nonrecurrent) and by PAM to classify categories and to identify genes that best characterize each class. SAM analysis was done using the R package ''samr'' as described previously (41). The list of ranked genes obtained was 203 genes in normal versus cancer (δ, 1.098; false discovery rate, 0.046) and 98 genes in recurrent versus nonrecurrent (δ, 1.338; false discovery rate, 0). Max T test was done in the Multtest package, module of Bioconductor R, according to the Westfall and Young method (42). PAM R supervised class prediction package was done as described in ref. 43. The performance of computational algorithm was tested by the k-fold cross-validation procedure for estimating generalization error based on resampling as described (44, 45). Regulated biological processes and molecular functions were identified by the GOAL Web-based application (46) and the Unigene Build 154 according to the Gene Ontology (GO; http://www.geneontology.org) Consortium classification. Briefly, for each GO term(s) associated to the Unigene cluster in the expression tables, mean t score from the t scores of each corresponding Unigene cluster was calculated. The Unigene clusters t scores were averaged when more genes were present for a single Unigene cluster. To provide a Ps for each GO term and false discovery rate, bootstrap analysis (44, 45) was done on data set generating a bootstrap resampling up to 1.25×10^6 total data. GO terms with Ps < 0.01 were considered differentially regulated. False discovery rate was calculated as described (47, 48). In particular, with a bootstrap of 25 cycles (for a total of 4.5×10^5 generated t score), the false discovery rate was 0.013 for up-regulated and 0.040 for down-regulated terms.

Adenoviral Infection and Terminal Deoxunucleotidyl Transferase–Mediated dUTP Nick End Labeling Assay

Replication-deficient recombinant adenovectors encoding the cDNA for human AdAKTdn (49) or no gene (AdNull) were prepared as described (50) and used at a multiplicity of infection of 50 plaque-forming units/cell. After infection, cells were starved in serum-deprived medium for 48 to 96 hours. Cells ($\sim 4 \times 10^4$) were cytocentrifuged onto glass slides and cytospin preparations were incubated for terminal deoxunucleotidyl transferase–mediated dUTP nick end labeling reaction (Boehringer Mannheim Italia S.p.A., Milan, Italy) and counterstained with Hoechst. Apoptosis was quantitated by determining the percentage of terminal deoxunucleotidyl transferase–mediated dUTP nick end labeling–positive cells within a field of view at a magnification of ×40. A total of 20 randomly chosen fields were counted for each slide and total counts were averaged to obtain the apoptotic index.

Statistical Analysis

Differences among subject groups were assessed by ANOVA, Student's t test, Mann-Whitney test, and Fisher's exact test. A 95% confidence interval ($P < 0.05$) was considered significant.

Acknowledgments

We thank Silvia Soddu for critical reading of the article, Claudia Colussi for excellent technical assistance, all members of the Division of Radiotherapy, Regina Elena Cancer Institute for helpful discussions, and Damiano Abeni for help with statistical analysis.

References

1. Gleason DF. Classification of prostatic carcinomas. Cancer Chemother Rep 1966;50:125–8.

2. Jewett HJ. The present status of radical prostatectomy for stages A and B prostatic cancer. Urol Clin North Am 1975;2:105–24.

3. Stamey TA, Yang N, Hay AR, McNeal JE, Freiha FS, Redwine E. Prostate-specific antigen as a serum marker for adenocarcinoma of the prostate. N Engl J Med 1987;317:909–16.

4. Singh D, Febbo PG, Ross K, et al. Gene expression correlates of clinical prostate cancer behavior. Cancer Cell 2002;1:203–9.

5. Dhanasekaran SM, Barrette TR, Ghosh D, et al. Delineation of prognostic biomarkers in prostate cancer. Nature 2001;412:822–6.

6. Glinsky GV, Glinskii AB, Stephenson AJ, Hoffman RM, Gerald WL. Gene expression profiling predicts clinical outcome of prostate cancer. J Clin Invest 2004;113:913–23.

7. Luo J, Duggan DJ, Chen Y, et al. Human prostate cancer and benign prostatic hyperplasia: molecular dissection by gene expression profiling. Cancer Res 2001; 61:4683–8.

8. Yu YP, Landsittel D, Jing L, et al. Gene expression alterations in prostate cancer predicting tumor aggression and preceding development of malignancy. J Clin Oncol 2004;22:2790–9.

9. Rubin MA, De Marzo AM. Molecular genetics of human prostate cancer. Mod Pathol 2004;17:380–8.

10. Peehl DM. Are primary cultures realistic models of prostate cancer? J Cell Biochem 2004;91:185–95.

11. Abate-Shen C, Shen MM. Molecular genetics of prostate cancer. Genes Dev 2000;14:2410–34.

12. Peehl DM. Primary cell cultures as models of prostate cancer development. Endocr Relat Cancer 2005;12:19–47.

13. He WW, Sciavolino PJ, Wing J, et al. A novel human prostate-specific, androgen-regulated homeobox gene (NKX3.1) that maps to 8p21, a region frequently deleted in prostate cancer. Genomics 1997;43:69–77.

14. Di Lorenzo G, Tortora G, D'Armiento FP, et al. Expression of epidermal growth factor receptor correlates with disease relapse and progression to androgen-independence in human prostate cancer. Clin Cancer Res 2002; 8:3438–44.

15. Tsuchiya N, Slezak JM, Lieber MM, Bergstralh EJ, Jenkins RB. Clinical significance of alterations of chromosome 8 detected by fluorescence *in situ* hybridization analysis in pathologic organ-confined prostate cancer. Genes Chromosomes Cancer 2002;34:363–71.

16. Isaacs W, De Marzo A, Nelson WG. Focus on prostate cancer. Cancer Cell 2002;2:113–6.

17. Hanahan D, Weinberg RA. The hallmarks of cancer. Cell 2000;100:57–70.

18. Sommerfeld HJ, Meeker AK, Piatyszek MA, Bova GS, Shay JW, Coffey DS. Telomerase activity: a prevalent marker of malignant human prostate tissue. Cancer Res 1996;56:218–22.

19. Fong CJ, Sherwood ER, Sutkowski DM, et al. Reconstituted basement membrane promotes morphological and functional differentiation of primary human prostatic epithelial cells. Prostate 1991;19:221–35.

20. Garraway LA, Lin D, Signoretti S, et al. Intermediate basal cells of the prostate: *in vitro* and *in vivo* characterization. Prostate 2003;55:206–18.

21. Sobel RE, Sadar MD. Cell lines used in prostate cancer research: a compendium of old and new lines. Part 2. J Urol 2005;173:360–72.

22. Sobel RE, Sadar MD. Cell lines used in prostate cancer research: a compendium of old and new lines. Part 1. J Urol 2005;173:342–59.

23. Ko D, Gu Y, Yasunaga Y, et al. A novel neoplastic primary tumor-derived human prostate epithelial cell line. Int J Oncol 2003;22:1311–7.

24. Paez J, Sellers WR. PI3K/PTEN/AKT pathway. A critical mediator of oncogenic signaling. Cancer Treat Res 2003;115:145–67.

25. Dairkee SH, Ji Y, Ben Y, Moore DH, Meng Z, Jeffrey SS. A molecular "signature" of primary breast cancer cultures; patterns resembling tumor tissue. BMC Genomics 2004;5:47.

26. Calvo A, Xiao N, Kang J, et al. Alterations in gene expression profiles during prostate cancer progression: functional correlations to tumorigenicity and down-regulation of selenoprotein-P in mouse and human tumors. Cancer Res 2002; 62:5325–35.

27. Jetzt A, Howe JA, Horn MT, et al. Adenoviral-mediated expression of a kinase-dead mutant of Akt induces apoptosis selectively in tumor cells and suppresses tumor growth in mice. Cancer Res 2003;63:6697–706.

28. van der Poel HG. Smart drugs in prostate cancer. Eur Urol 2004;45:1–17.

29. Hidalgo M. New target, new drug, old paradigm. J Clin Oncol 2004; 22:2270–2.

30. Majumder PK, Febbo PG, Bikoff R, et al. mTOR inhibition reverses Akt-dependent prostate intraepithelial neoplasia through regulation of apoptotic and HIF-1-dependent pathways. Nat Med 2004;10:594–601.

31. Bartkova J, Horejsi Z, Koed K, et al. DNA damage response as a candidate anti-cancer barrier in early human tumorigenesis. Nature 2005;434:864–70.

32. Gorgoulis VG, Vassiliou LV, Karakaidos P, et al. Activation of the DNA damage checkpoint and genomic instability in human precancerous lesions. Nature 2005;434:907–13.

33. Gu W, Malik S, Ito M, et al. A novel human SRB/MED-containing cofactor complex, SMCC, involved in transcription regulation. Mol Cell 1999; 3:97–108.

34. Li S, Huang S, Peng SB. Overexpression of G protein-coupled receptors in cancer cells: involvement in tumor progression. Int J Oncol 2005;27:1329–39.

35. Semenza GL. Targeting HIF-1 for cancer therapy. Nat Rev Cancer 2003;3: 721–32.

36. Cianciulli AM, Leonardo C, Guadagni F, et al. Genetic instability in superficial bladder cancer and adjacent mucosa: an interphase cytogenetic study. Hum Pathol 2003;34:214–21.

37. Kim NW, Wu F. Advances in quantification and characterization of telomerase activity by the telomeric repeat amplification protocol (TRAP). Nucleic Acids Res 1997;25:2595–7.

38. Nanni S, Narducci M, Della Pietra L, et al. Signaling through estrogen receptors modulates telomerase activity in human prostate cancer. J Clin Invest 2002;110:219–27.

39. Uzgare AR, Xu Y, Isaacs JT. *In vitro* culturing and characteristics of transit amplifying epithelial cells from human prostate tissue. J Cell Biochem 2004; 91:196–205.

40. Nakatani K, Thompson DA, Barthel A, et al. Up-regulation of Akt3 in estrogen receptor-deficient breast cancers and androgen-independent prostate cancer lines. J Biol Chem 1999;274:21528–32.

41. Tusher VG, Tibshirani R, Chu G. Significance analysis of microarrays applied to the ionizing radiation response. Proc Natl Acad Sci U S A 2001; 98:5116–21.

42. Westfall PH, Young SS. Resampling-based multiple testing: examples and methods for *P*-value adjustment. New York: Wiley; 1993.

43. Tibshirani R, Hastie T, Narasimhan B, Chu G. Diagnosis of multiple cancer types by shrunken centroids of gene expression. Proc Natl Acad Sci U S A 2002; 99:6567–72.

44. Efron B, Tibshirani R. An introduction to the bootstrap. New York: Chapman and Hall/CRC;1993.

45. Hastie T, Tibshirani R, Friedman J. The elements of statistical learning. Data mining, interference and prediction. New York:Springer;2001.

46. Volinia S, Evangelisti R, Francioso F, Arcelli D, Carella M, Gasparini P. GOAL: automated Gene Ontology analysis of expression profiles. Nucleic Acids Res 2004;32:W492–9.

47. Reiner A, Yekutieli D, Benjamini Y. Identifying differentially expressed genes using false discovery rate controlling procedures. Bioinformatics 2003; 19:368–75.

48. Efron B, Tibshirani R. Empirical Bayes methods and false discovery rates for microarrays. Genet Epidemiol 2002;23:70–86.

49. Fujio Y, Walsh K. Akt mediates cytoprotection of endothelial cells by vascular endothelial growth factor in an anchorage-dependent manner. J Biol Chem 1999;274:16349–54.

50. Gowdak LH, Poliakova L, Wang X, et al. Adenovirus-mediated VEGF(121) gene transfer stimulates angiogenesis in normoperfused skeletal muscle and preserves tissue perfusion after induction of ischemia. Circulation 2000; 102:565–71.

51. Chung CH, Parker JS, Karaca G, et al. Molecular classification of head and neck squamous cell carcinomas using patterns of gene expression. Cancer Cell 2004;5:489–500.

52. Welsh JB, Sapinoso LM, Su AI, et al. Analysis of gene expression identifies candidate markers and pharmacological targets in prostate cancer. Cancer Res 2001;61:5974–8.

Molecular Cancer Research

Epithelial-Restricted Gene Profile of Primary Cultures from Human Prostate Tumors: A Molecular Approach to Predict Clinical Behavior of Prostate Cancer

Simona Nanni, Carmen Priolo, Annalisa Grasselli, et al.

Mol Cancer Res 2006;4:79-92.